

Supporting Information

Article title: Plant hydraulic traits regulating productivity and drought resistance in boreal crops

Authors: Hui Tang, Samuli Launianen, Julius Vira, Liisa Kulmala, Palosuo Taru, Aaltonen Hermanni, Olli Nevalainen, Istem Fer, Henriikka Vekuri, Jari-Pekka Nousu, Mika Korkiakoski, Jari Liski

The following Supporting Information is available for this article:

Table S1: List of input variables for SPY-C.

Table S2: List of model parameters for SPY-C.

Table S3: Summary of available measurements of hydraulic traits for different crops.

Fig. S1: Soil moisture simulated by SPY-C and its comparison with observation.

Fig. S2: Soil measurements at Hauho and the estimation of soil carbon stock for 0-1 meter depth.

Fig. S3: The effect of α on J_{cmax} , and γ on $\Delta\psi$.

Fig. S4: The best-fit PPEs members of QV_swrc3 and their performances.

Fig. S5: The ensemble spread of the PPE of QV_swrc3

Fig. S6: Morris's sensitivity analysis using the PPE of QV_swrc3

Fig. S7: The comparison of daily snow depth in ERA5-land, SPY-C with observation.

Fig. S8: The assessment of isohydricity and critical soil moisture threshold at the GRASS and OAT site

Fig. S9: The stomatal safety margin deduced by SPY-C for the forage grass at the GRASS site.

Fig. S10: Morris's sensitivity analysis using the PPE of QV_fullSM and HA_fullSM.

Fig. S11: Morris's sensitivity analysis using the PPE of QV_noVPD and HA_noVPD..

Fig. S12: The performance of SPY-C in simulating net ecosystem exchange (NEE).

Methods S1: Phenology and allocation module of SPY-C

Methods S2: Input and output of SPY-C.

Methods S3: Analyses of root-zone available water at Qvidja and Hauho.

Methods S4: The algorithm for selecting the best-fit PPE members using different benchmarking time periods.

Table S1: List of input variables for SPY-C.

Fields (Units)	ResolutionRequired?		Fields (Units)	Resolution	Required?
Air temperature T (K)	Hourly	Yes	CO2 concentration (mol mol-1)	Hourly	Yes
Precipitation flux P (kg m-2 s-1)	Hourly	Yes	Leaf area index LAI (m2 m-2)	Daily	Optional
Surface downwelling shortwave flux R_g (W/m2)	Hourly	Yes	Volumetric soil moisture (m3 m-3)	hourly	Optional
Relative_humidity q_r (%)	Hourly	Yes	Management type	Daily	Optional
Air pressure P_{atm} (Pa)	Hourly	Yes	C input due to management (kg C m-2 s-1)	Daily	Optional
Wind speed (m s-1)	Hourly	Yes	C output due to mangement (kg C m-2 s-1)	Daily	Optional

Table S2: List of model parameters for SPY-C and the values used in this study.

Code name	Parameter name	Description	units	Qvidja	Hauho
P-hydro					
pft_type		Type of plant or crop		"grass"	"oat"
conductivity	K_p	Maximum whole-plant conductance per unit leaf area.	m	see Table 1	see Table 1
psi50	ψ_{50}	Water potential at which 50 conductivity is lost.	Pa	see Table 1	see Table 1
b	b	Shape parameters of vulnerability curve	-	2	2
rdark	r_{dark}	Dark respiration rate per unit carboxylation capacity	-	0.015	0.015
alpha	α	Unit cost of photosynthetic capacity	-	see Table 1	see Table 1
gamma	γ	Unit cost of maintaining the hydraulic pathway	$mol m^{-2} s^{-1} Pa^{-2}$	see Table 1	see Table 1
Opt_hypothesis		Optimization hypothesis, PM: profit maximization; "LC": least cost.	-	"PM"	"PM"
SpaFHy					
soil_depth		Root zone depth	m	0.6	0.6
max_poros		Soil porosity	$m^3 m^{-3}$	0.46 (0.54)	0.47
fc		Field capacity	$m^3 m^{-3}$	0.36 (0.29)	0.16
wp		Wilting point	$m^3 m^{-3}$	0.22 (0.09)	0.04
n_van	n	Empirical shape parameter in Van Genuchten model	-	1.07 (1.18)	1.27
watres	θ_r	Residual water content	$m^3 m^{-3}$	0	0
alpha_van	α_v	Empirical shape parameter in Van Genuchten model	-	2.02 (3.35)	4.49
ksat	K_{sat}	Hydraulic conductivity at saturation	ms^{-1}	$2.00e^{-6}$	$2.00e^{-6}$
wmax		Storage capacity for rain	mm/LAI	0.5	0.5
wmaxsnow		Storage capacity for snow	mm/LAI	4.5	4.5
maxpond		Max ponding storage	mm	0	0
hc		Canopy height	m	0.6	0.6
w_leaf		Leaf length scale	m	0.01	0.01
gsoil		Soil surface conductance if soil is fully wet	m/s	$5.00e^{-3}$	$5.00e^{-3}$
kmelt		Melt coefficient	mm/s	$2.89e^{-5}$	$2.89e^{-5}$
kfreeze		Freezing coefficient	mm/s	$5.79e^{-6}$	$5.79e^{-6}$
frac_snowliq		Maximum fraction of liquid in snow	-	0.05	0.05
zmeas		Wind speed measurement height above canopy	m	2	2
zground		Height above ground where ground wind speed is computed	m	0.1	0.1
zo_ground		Forest floor roughness length	m	0.01	0.01
Phenology Allocation					

Code name	Parameter name	Description	units	Qvidja	Hauho
cratio_leaf	a_{leaf}	Proportion of primary production allocated to leaf.	-	inferred from LAI	inferred from LAI
cratio_root	a_{root}	Proportion of primary production allocated to leaf and root.	-	inferred from LAI	inferred from LAI
cratio_resp	m_r	Base maintenance respiration ratio at 20°C.	$s^{-1}m^{-2}$	$5.00e^{-8}$	$5.00e^{-8}$
cratio_gr_resp	g_r	Growth respiration ratio.	-	0.11	0.11
cratio_biomass	r_c	Carbon content of leaf biomass	-	0.42	0.42
turnover_cleaf	k_{leaf}	Leaf turnover rates.	day^{-1}	0.03	0.03
turnover_croot	k_{root}	Root turnover rates.	day^{-1}	0.004	0.004
sla	SLA	Specific leaf area.	m^2kg^{-1}	10	10
q10	Q_{10}	Q_{10} temperature coefficient.	-	2	2
harvest_index		Harvest index	-	0.8	0.8
invert_option		Options to inversely calculate leaf allometric ratio (1) or turnover rate (2) from LAI	-	1	1
YASSO					
awenh_fineroor		Fractionation of organic carbon into acid-hydrolysable (A), water (W) and ethanol (E) soluble and insoluble (N) and humus (H) fractions (AWENH) of fine root.	-	0.46, 0.32, 0.04, 0.18, 0.0	0.71, 0.08, 0.03, 0.18, 0.0
awenh_leaf		AWENH composition of leaf.	-	0.46, 0.32, 0.04, 0.18, 0.0	0.46, 0.32, 0.04, 0.18, 0.0
awenh_soluble		AWENH composition of soil amendment containing soluble carbon.	-	0.0, 1.0, 0.0, 0.0, 0.0	0.0, 1.0, 0.0, 0.0, 0.0
awenh_compost		AWENH composition of organic fertilizer, i.e., manure.	-	0.69, 0.09, 0.02, 0.20, 0.0	0.69, 0.09, 0.02, 0.20, 0.0
tempr_c		Climatological mean annual temperature.	$^{\circ}C$	5.67	4.5
tempr_ampl		Annual amplitude of monthly mean temperature.	$^{\circ}C$	23.5	26.0
precip_day		Climatological mean precipitation.	$mm\ day^{-1}$	1.76	1.58
totc		Total soil organic carbon at initialization stage	$kgC\ m^{-2}$	16	12
fract_root_input		Fraction of input C with the fineroor composition	-	0.4	0.4
fract_legacy_soc		Fraction of humus carbon pool assumed at initialization.	-	0.3	0.1
alpha_smooth_temp		Exponential smoothing factor for temperature.	-	0.01	0.01

Code name	Parameter name	Description	units	Qvidja	Hauho
alpha_smooth_pre		Exponential smoothing factor for precipitation.	-	0.0016	0.0016

Table S3: Summary of available measurements of hydraulic traits for different crops.

Species	Veg. types	Region of study	Organs	$K_{max}(nmolm^{-2}s^{-1}MPa^{-1})$	$K_{max}(10^{-6}m)$	$\psi_{50}(MPa)$	Stomatal safety margin ($\psi_{gs90} - \psi_{50}$) ^a	methods	References
<i>Lolium multiflorum</i> - Barberia	Annual or biennial ryegrass (C3)	Temperate	Leaf	47.97	8.63	-1.14	0.11	Glasshouse	Holloway-Phillips and Brodribb (2011a)
<i>Lolium multiflorum</i> - Feast	Annual or biennial ryegrass (C3)	Temperate	Leaf	50.59	9.1	-1.07	-0.21	Glasshouse	Holloway-Phillips and Brodribb (2011a)
<i>Festuca arundinacea</i> - Quantum	Perennial bunchgrass (C3)	Temperate	Leaf	31.67	5.7	-1.03	-0.9	Glasshouse	Holloway-Phillips and Brodribb (2011a)
<i>Festuca arundinacea</i> - Flecha	Perennial bunchgrass (C3)	Temperate	Leaf	19.56	3.52	-1.14	-0.95	Glasshouse	Holloway-Phillips and Brodribb (2011a)
<i>Lolium perenne</i> L.	Perennial ryegrass (C3)	Temperate	Leaf	15	2.7	-1	-1.35	Glasshouse	Holloway-Phillips and Brodribb (2011b)
<i>Festuca arundinacea</i> - fescue	Perennial bunchgrass (C3)	Temperate	Leaf	5.99	1.08	-2.3	-0.92	field experiment	Jacob et al. (2022)
<i>Phalaris aquatica</i>	Perennial grass (C3)	Temperate	Leaf	5.34	0.96	-1.78	-1.19	field experiment	Jacob et al. (2022)
<i>Chloris gayana</i>	Perennial grass (C4)	Tropical	Leaf	3.95	0.711	-1.83	-1.81	field experiment	Jacob et al. (2022)
<i>Digitaria eriantha</i>	Perennial grass (C4)	Tropical	Leaf	3.93	0.71	-1.31	-1.83	field experiment	Jacob et al. (2022)
<i>Themeda triandra</i>	Perennial grass (C4)	Tropical	Leaf	5.43	0.9774	-2.08	-2.99	field experiment	Jacob et al. (2022)
<i>Triticum aestivum</i> - SY Mattis	Annual, Wheat (C3)	Temperate	Leaf	38.41	6.91	-1 (-2.2/-2.4) ^b	-0.38	Laboratory	Corso et al. (2020)
<i>Triticum aestivum</i> - Heron	Annual, Wheat (C3)	Temperate	Leaf			-2.87		Laboratory	Johnson et al. (2018)
<i>Solanum lycopersicum</i> - Ailsa Craig	Annual, Tomato (C3)	Temperate	Stem	61.11	11.00	-2.55	1.6	Laboratory	Lamarque et al. (2020)
<i>Solanum lycopersicum</i> - Transgenic line (overexpresses ABA)	Annual, Tomato (C3)	Temperate	Stem	41.67	7.50	-1.99	1.03	Laboratory	Lamarque et al. (2020)
<i>Solanum lycopersicum</i> - Rhineland's Rhun	Annual, Tomato (C3)	Temperate	Leaf	4	0.72	-1.54	0.5	glasshouse	Skelton et al. (2017)
<i>Helianthus annuus</i> - Melody	Annual, Sunflower (C3)	Temperate	Stem	8.89	1.60	-3.09		Laboratory	Ahmad et al. (2018)
<i>Helianthus annuus</i> - ES_Biba	Annual, Sunflower (C3)	Temperate	Stem	7.78	1.40	-2.67		Laboratory	Ahmad et al. (2018)
<i>Helianthus annuus</i> - ES_Ethic	Annual, Sunflower (C3)	Temperate	Stem	13.33	2.40	-3.22		Laboratory	Ahmad et al. (2018)
<i>Helianthus annuus</i> - LG_5660	Annual, Sunflower (C3)	Temperate	Stem	9.44	1.70	-3.01		Laboratory	Ahmad et al. (2018)
<i>Phaseolus vulgaris</i> -G4523 and Othello	Annual, Bean (C3)	Temperate	Stem			-0.4 - -1.0		Laboratory	Matzner et al. (2014)
<i>Phaseolus vulgaris</i> -Othello and Durango race	Annual, Bean (C3)	Temperate	Stem	13.89 (7.78) ^c	2.50 (1.4) ^c	-0.37 - -0.66		Laboratory	Holste et al. (2006)
<i>Glycine max</i> (ten cultivars)	Annual, Soybean (C3)	Temperate	Stem			-1.4 - -2.4		Laboratory	Schell et al. (2025)
<i>Pisum sativum</i> L. - Alvesta	Annual, Pea (C3)	Temperate	Stem			-2.84 - -3.11		field experiment	Sun et al. (2021)
<i>Hordeum vulgare</i> L. - Eunova	Annual, Barley (C3)	Temperate	Stem			-2.04 - -2.92		field experiment	Sun et al. (2021)
<i>Avena sativa</i> - Flega (susceptible to drought)	Annual, Oat (C3)	Temperate	Root	33.33	6.00	-1.3	0.1	Laboratory	Canales et al. (2021)
<i>Avena sativa</i> - Patones (resistant to drought)	Annual, Oat (C3)	Temperate	Root	44.44	8.00	-1.6	0.6	Laboratory	Canales et al. (2021)
<i>Zea mays</i> L.	Annual, Maize (C4)	Temperate	Leaf	31.45	5.66	-0.85	>=-0.77	Field experiment	Gleason et al. (2021)
<i>Phleum pratense</i> , <i>Festuca pratensis</i> , <i>Trifolium repens</i>	Perennial, Bunchgrass (C3)	Boreal	Whole plant		0.5	-1 - -3	-0.2 - -0.6	Model-flux inversion	This study
<i>Avena sativa</i>	Annual, Oat (C3)	Boreal	Whole plant		0.5	-1 - -3		Model-flux inversion	This study
<i>Lolium multiflorum</i>	Annual, ryegrass (C3)	Boreal	Whole plant		3.7 - 6.8	-1 - -3		Model-flux inversion	This study

^a ψ_{gs90} is leaf water potential at which 90% stomatal closure is observed.
^b Values in parenthesis are from different methods (centrifuge vs. image of embolism).
^c Values in parenthesis are for different soil types.

Fig. S1: Soil moisture simulated by SPY-C and its comparison with observation. Observed soil moisture for Qvidja (a, b) is from 5 cm soil depth, and is from 10 cm soil depth for Hauho (10 cm). Modelled soil moisture represent the whole root zone and is from the best-fit PPE members of QV_ctrl (Qvidja) and HA_ctrl (Hauho), respectively. The dynamics of simulated soil moisture for the root zone is consistent with that of the observed soil moisture at surface level.

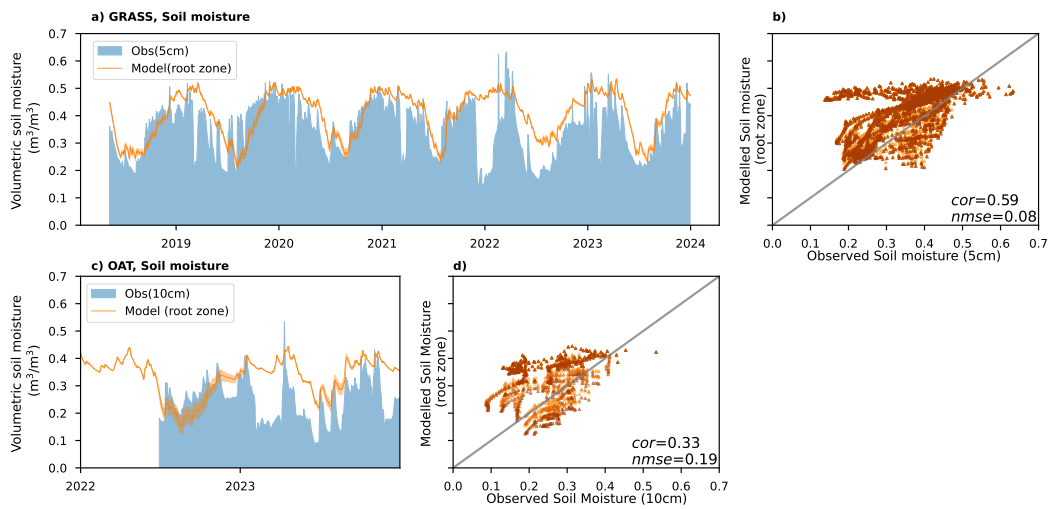


Fig. S2: Soil measurements at Hauho and the estimation of soil carbon stock for 0-1 meter depth. There were in total 15 soil cores taken from the site in 2024. Each core reached to 50 cm soil depth when possible, and soil organic carbon content and bulk density were measured for each 10 cm intervals. All the measurements were performed by Cense Analytics Oy. Different colors and symbols in the figure denote the results from different soil cores. It was found that the accumulative carbon storage of each soil core follows a logarithmic relation with soil depth very well. This allows us to extrapolate soil carbon stock to 1 meter depth with reasonably accuracy.

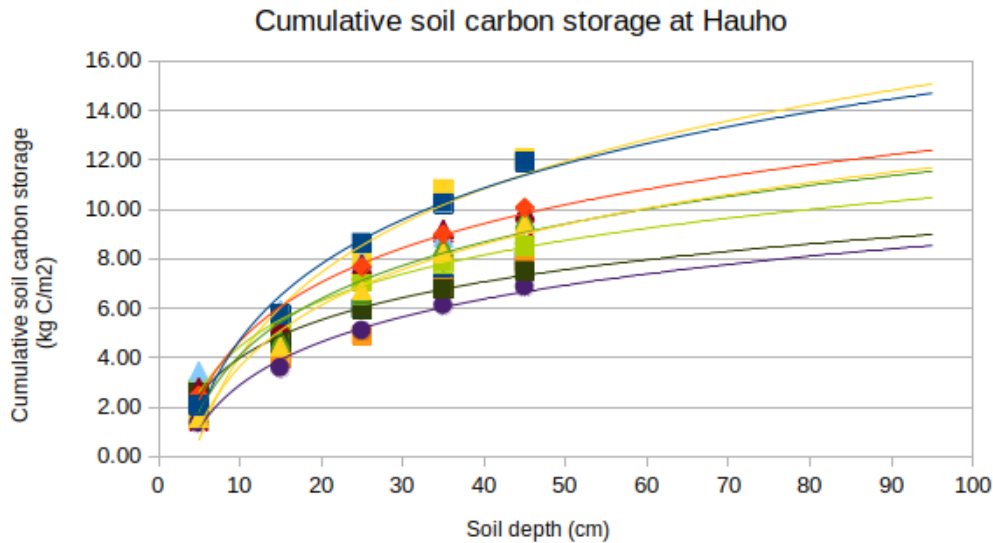


Fig. S3: Probability density function of J_{cmax} (a, c) using different values of α and $\Delta\psi$ (b, d) using different values of γ for both GRASS site (a, b) and OAT site (c, d). The grey lines in the plots denote the probability density function that best fit the sites.

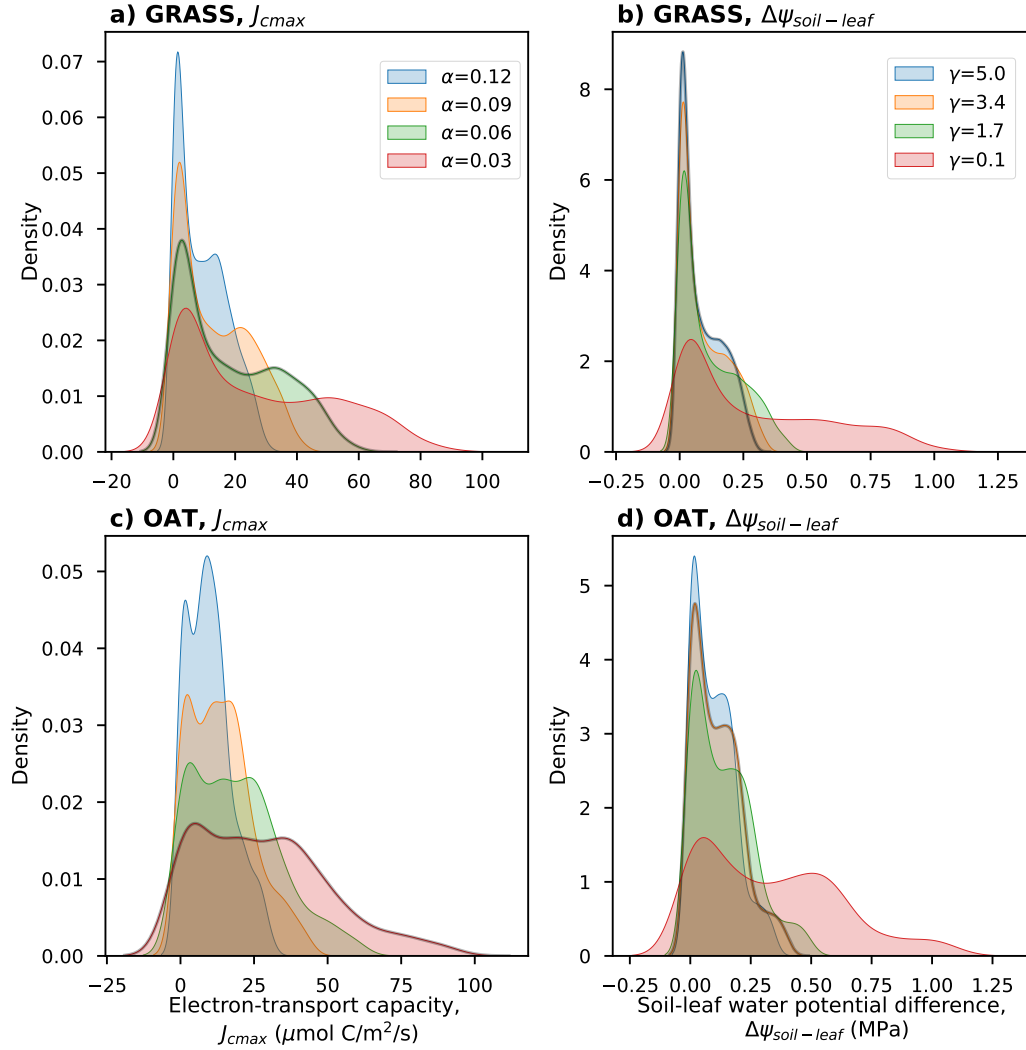


Fig. S4: The best-fit PPEs members of QV_swrc3 and their performances. (a-d) The best-fit parameter sets selected for Qvidja (QV_swrc3) based on different benchmarking time periods (Method S3). The positions of the 5 best-fit parameter sets selected using 01.2019-12.2022 as the benchmarking periods are denoted by cross signs, representing the main crops (i.e., forage grass) at Qvidja. (e-f) The simulated daily mean gross primary productivity (GPP), evapotranspiration (ET) and their comparison with the observation.

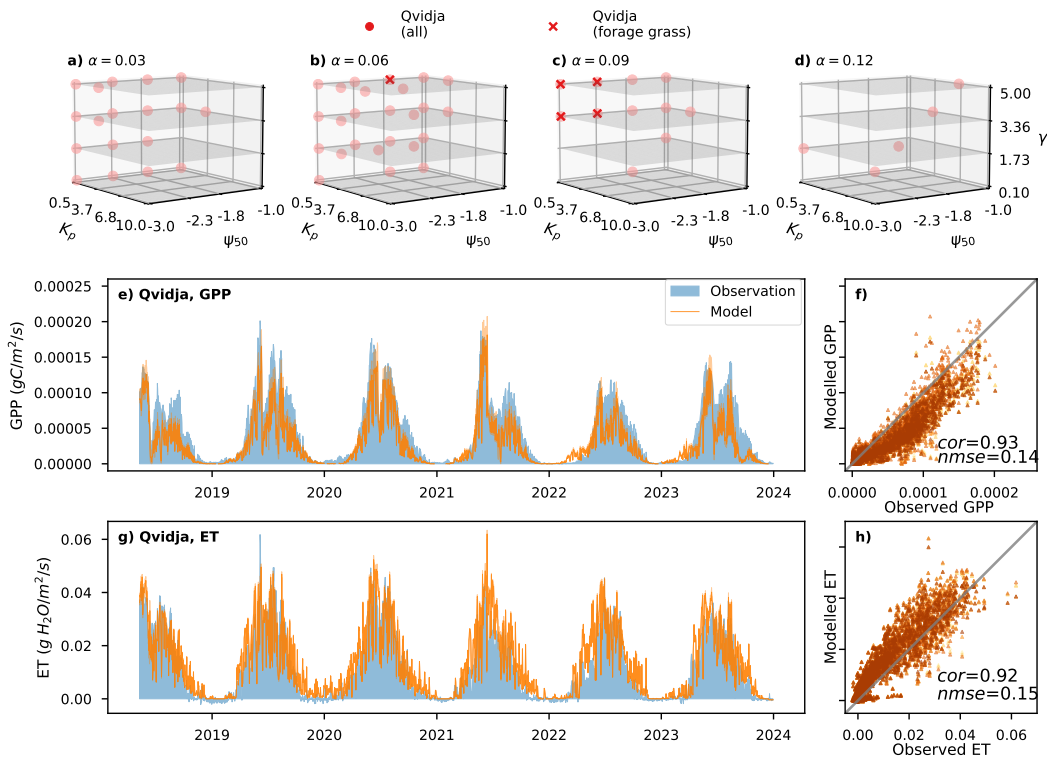


Fig. S5: The ensemble spread of the PPE of QV_swrc3. The violin plots showing the spread of monthly mean GPP (a), ET (b), water use efficiency at plant levels (pWUE) (c), internal water use efficiency (iWUE) (d), and soil moisture (e) in the PPE. The width of the violin denotes the probability density of the ensemble members that yield the same values. The red circles represent the mean value of the 5 best-fit PPE members. The red bars denote the observed values. The brown boxes in (e) denote meteorological drought months according to SPEI index (<-1.5). The dotted line in (e) denotes the wilting point.

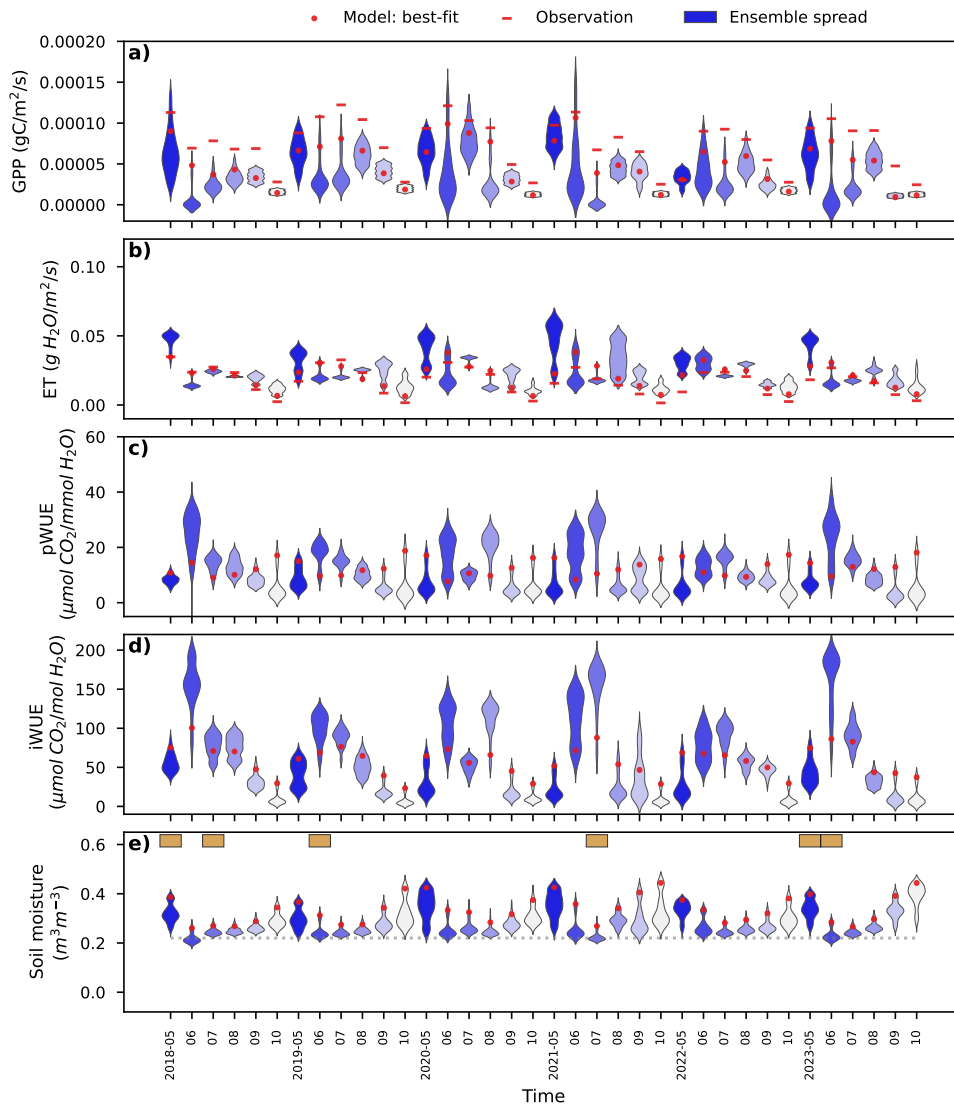


Fig. S6: Morris's sensitivity analysis using the PPE of QV_swrc3, including monthly averaged GPP (a), ET (b), plant-level water use efficiency (pWUE) (c), internal water use efficiency (iWUE) (d) and soil moisture (e) to Phydro parameters during growing season (May-October). The mean of the absolute elementary effect (MU^*) is denoted by the sized of the circle. The mean of the elementary effect (MU) is denoted by the colour shading of the circle. The standard deviation of the elementary effect ($Sigma$) is denoted by the colour shading of the rectangles.

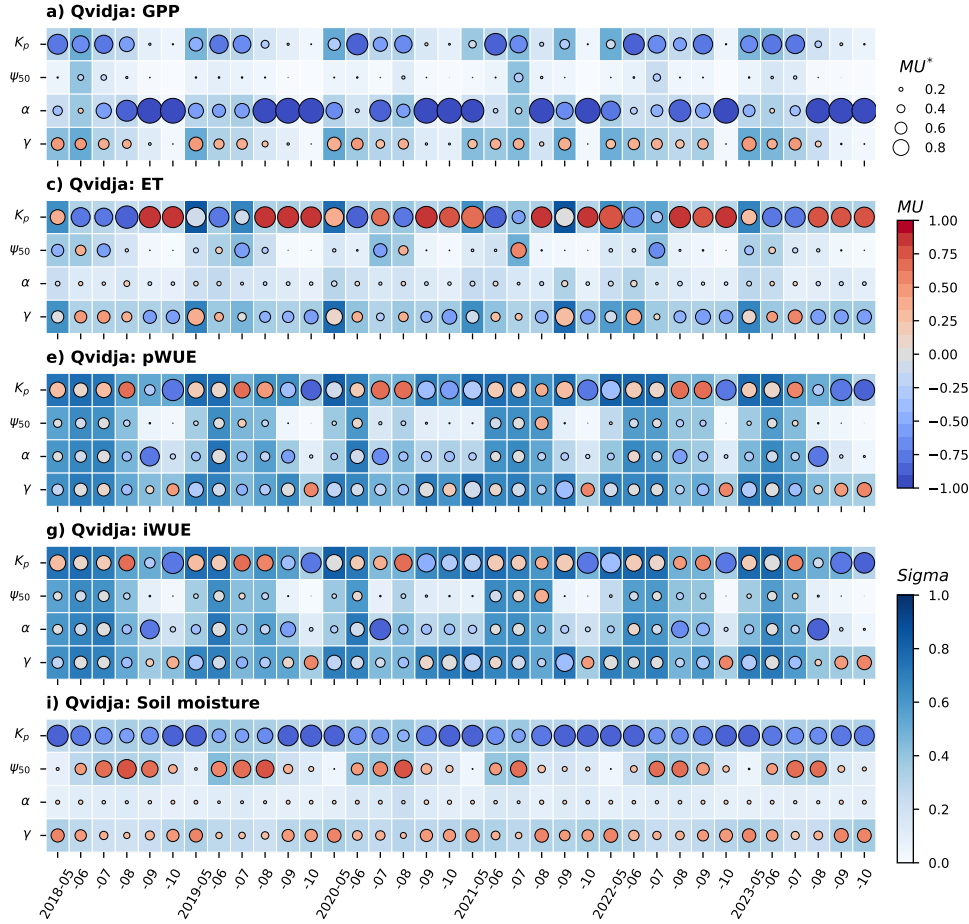
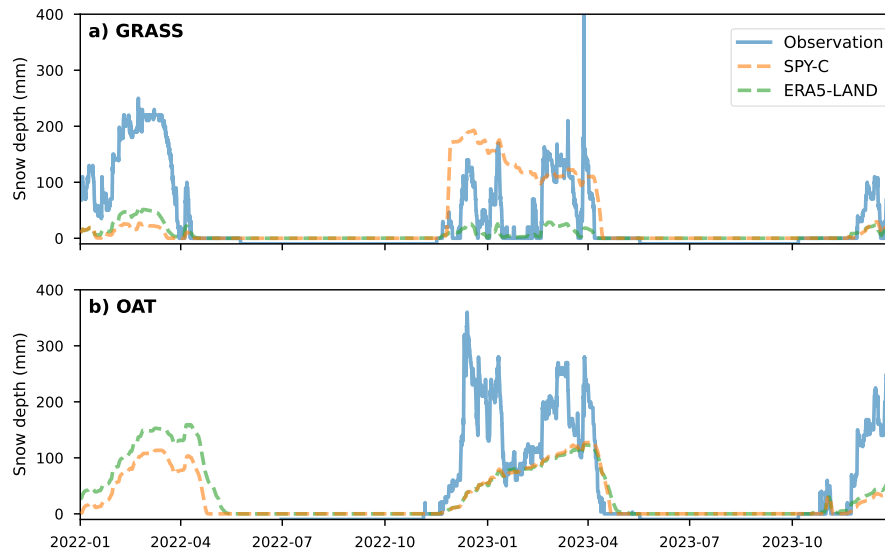
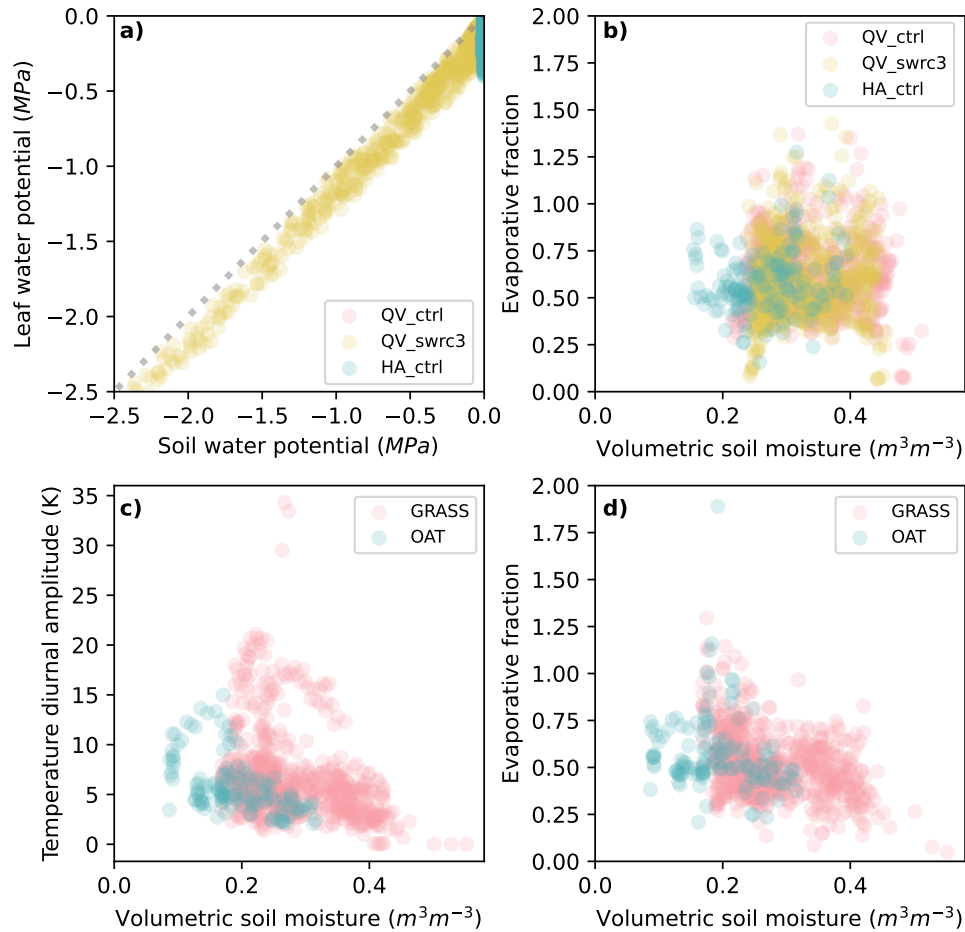


Fig. S7: Comparison of the daily snow depth (mm) in SPY-C, ERA5-land with the observation at Qvidja (a) and Hauho (b). For SPY-C and ERA5-land, snow water equivalent is used, which explains the lower values of both SPY-C and ERA5-land compared to observation.



70 **Fig. S8:** Modelled relation between leaf and soil water potential (a), and the assessment of critical soil moisture threshold (b) at the GRASS and OAT site using the results of the five best-fit PPE members selected from QV_ctrl, QV_swrc3 and HA_ctrl. The assessment of critical soil moisture threshold using observed diurnal temperature amplitude and evaporative fraction similar to that in the study by Fu et al. (2024) are shown in (c) and (d), respectively.



75 **Fig. S9:** The hydraulic safety margins deduced by SPY-C for the forage grass at the GRASS site. Each subplots represent the results from one of the five best-fit PPE members from QV_ctrl. ψ_{gs90} : the leaf water potential at which leaf loses 90% of its stomatal conductance. ψ_{50} : the leaf water potential at which leaf loses 50% of its hydraulic conductance. ψ_{min} : the minimum leaf water potential experienced by the plant during the model simulation years (2018-2023).

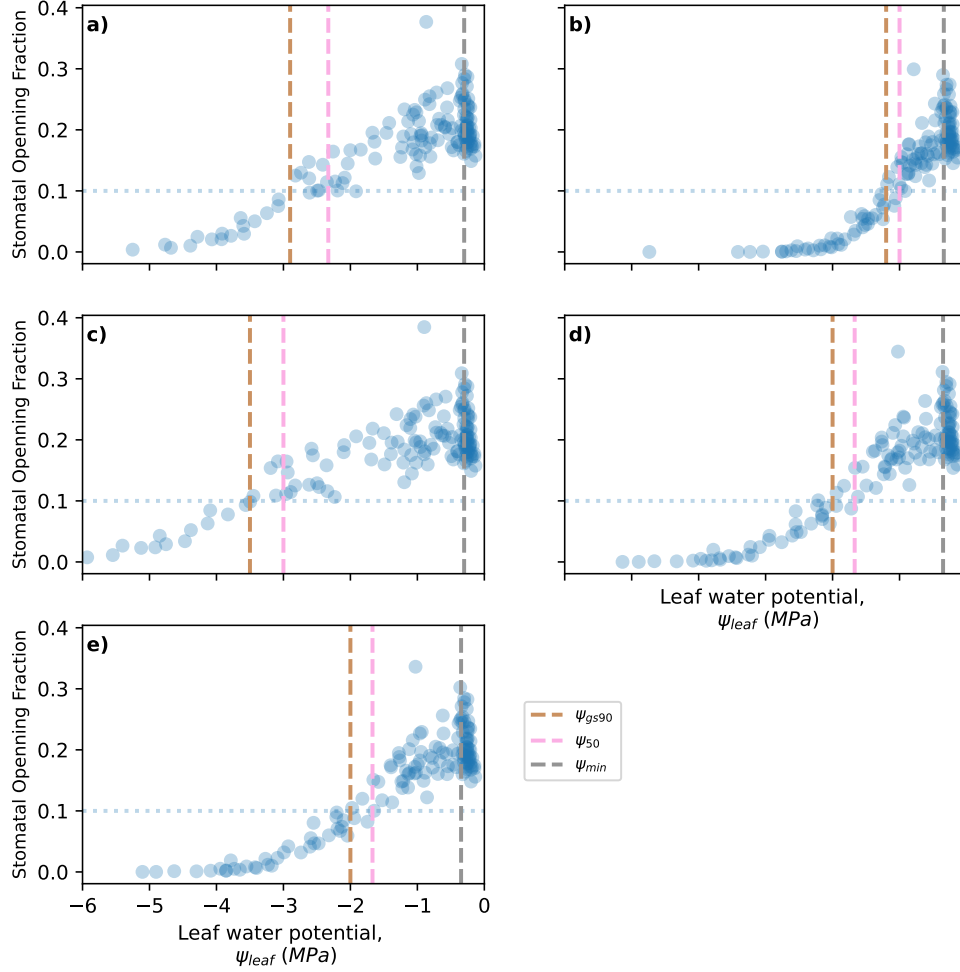


Fig. S10: Morris’s sensitivity analysis using the PPE of QV_fullSM and HA_fullSM.

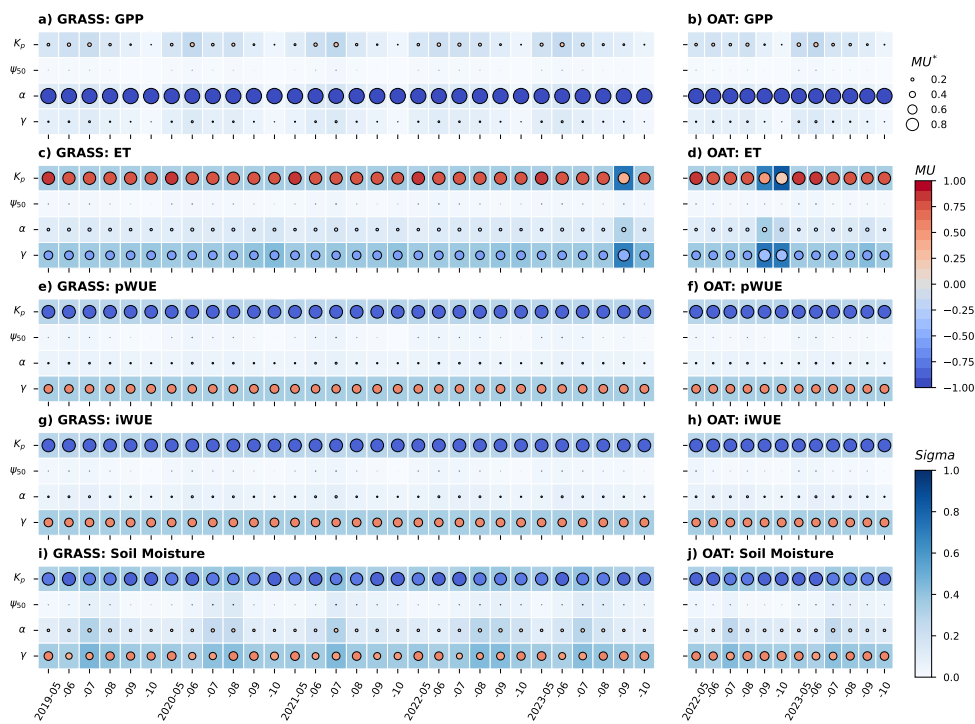


Fig. S11: Morris’s sensitivity analysis using the PPE of QV_noVPD and HA_noVPD.

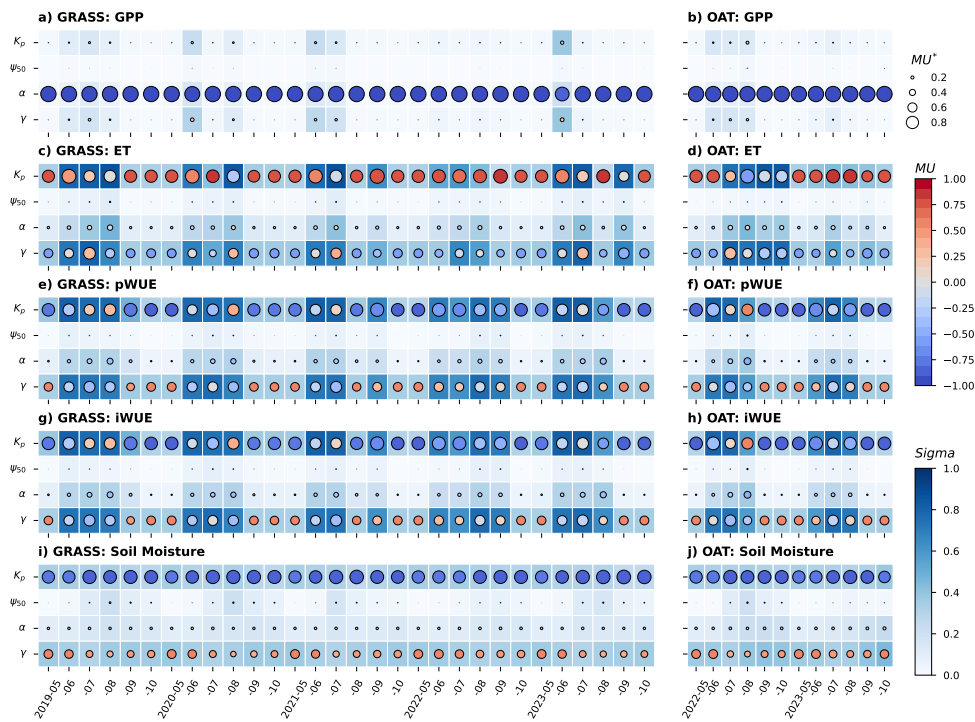
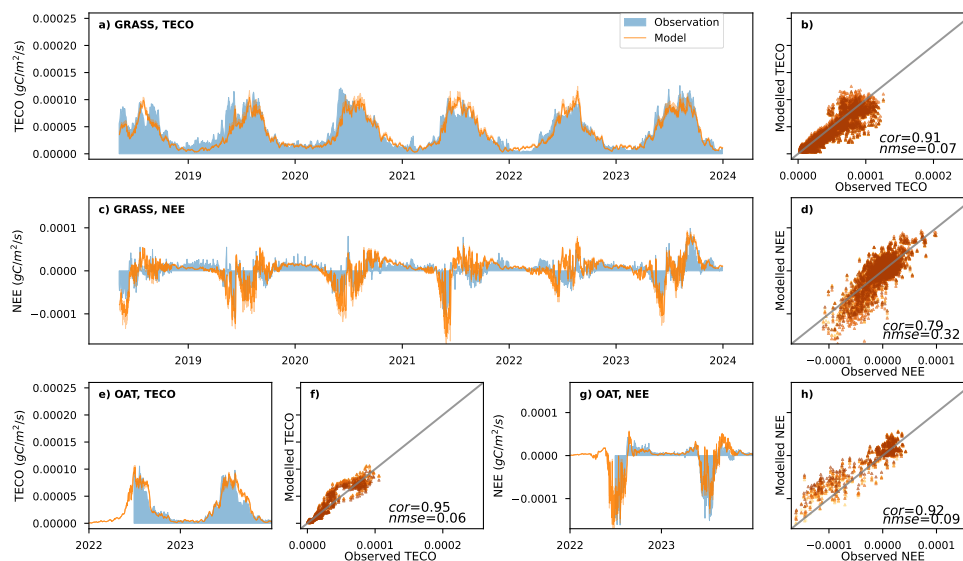


Fig. S12: The performance of SPY-C in simulating daily total ecosystem respiration (TECO) and net ecosystem exchange (NEE) at Qvidja (QV_ctrl) (a-d) and Hauho (HA_ctrl) (e-h).



Methods S1: Phenology and Allocation Module of SPY-C

85

For leaf, the maintenance respiration flux $CF_{mr,leaf}$ (unit: $kg\ m^{-2}d^{-1}$), i.e. leaf dark respiration, is proportional to the maximum carboxylation capacity (V_{cmax}) (Eq. S1) in line with the assumption in Phydro (Eq. 5). In contrast, the maintenance respiration of grain and root compartments ($CF_{mr,grain}$, $CF_{mr,root}$) is proportional to their carbon storage (CS_{grain} , CS_{root}) (Eq. S2 and S3).

$$90\ CF_{mr,leaf} = b_r \overline{V_{cmax}} \cdot LAI \quad (S1)$$

$$CF_{mr,root} = CS_{root} \cdot m_r \cdot Q_{10}^{(\overline{T}-20)/10} \quad (S2)$$

$$CF_{mr,grain} = CS_{grain} \cdot m_g \cdot Q_{10}^{(\overline{T}-20)/10} \quad (S3)$$

95 where $\overline{V_{cmax}}$ is the daily averaged carboxylation capacity, $Q_{10} = 2.0$ is the temperature coefficient for plant respiration (Rasmussen et al., 2019). The m_r and m_g is the base maintenance respiration ratio at 20 °C for root and grain, respectively. We assume $m_g = 0.1m_r$, reflecting lower maintenance respiration of the grain than that of root commonly found in the cereal crop. \overline{T} is the average temperature on the day.

100 The growth respiration of leaf ($CF_{gr,leaf}$), grain ($CF_{gr,grain}$) and root ($CF_{gr,root}$) is proportional to the newly available carbon for growth at each daily time step (Eq. S4, S5 and S6).

$$CF_{gr,leaf} = (CF_{gpp:leaf} - CF_{mr,leaf}) \cdot g_r \quad (S4)$$

$$CF_{gr,grain} = (CF_{gpp:grain} - CF_{mr,grain}) \cdot g_r \quad (S5)$$

$$105\ CF_{gr,root} = (CF_{gpp:root} - CF_{mr,root}) \cdot g_r \quad (S6)$$

where g_r is the growth respiration ratio, which is set to 0.11 similar to other models (Lombardozzi et al., 2020). Autotrophic respiration is the sum of maintenance and growth respiration of different plant components (Eq. S7).

$$AR = CF_{mr,leaf} + CF_{mr,root} + CF_{mr,grain} + CF_{gr,leaf} + CF_{gr,root} + CF_{gr,grain} \quad (S7)$$

110 In SPY-C, the litter carbon fluxes from leaf ($CF_{leaf:litter}$) and root ($CF_{root:litter}$) are described proportional to carbon storage and depend on temperature (Eq. S8 and S9).

$$CF_{leaf:litter} = CS_{leaf} \cdot k_{leaf} \cdot Q_{10}^{(\overline{T}-20)/10} \quad (S8)$$

$$CF_{root:litter} = CS_{root} \cdot k_{root} \cdot Q_{10}^{(\overline{T}-20)/10} \quad (S9)$$

where k_{leaf} and k_{root} are the leaf and root turnover rates, respectively.

115 The allocation ratios (a_{leaf} , a_{grain} and a_{root}) vary with plant phenology and environmental conditions, which is challenging to be described mechanistically (Xia et al., 2023; Westermann et al., 2024). Therefore, in this study, the observation-based daily LAI is used to inform leaf phenology and to constrain changes in leaf carbon storage according to Eq. S10. Changes in leaf allocation coefficients (a_{leaf}) can hence be deduced via the law of mass balance (see Eq. S11).

$$\Delta CS_{leaf} = \Delta LAI / SLA \cdot r_c \quad (S10)$$

120

$$a_{leaf} = (\Delta CS_{leaf} + CF_{leaf:litter} + CF_{mr,leaf} + CF_{gr,leaf}) / \overline{GPP} \quad (S11)$$

where ΔLAI is the change of LAI at each daily time step, SLA is the specific leaf area (unit: $m^2 \text{ kg}^{-1}$) of the plant and $r_c = 0.42$ is the carbon content of dry leaf biomass.

125 For cereal crops, the grain allocation coefficient (a_{grain}) is also prescribed using observed harvest date and yield. The grain filling period is assumed to start when the observed LAI reaches its maximum (d_{start}), and ends on the harvest date (d_{end}), similar to other models (clm, 2018). It is assumed that the accumulative grain filling flux ($CF_{gpp:grain}$) at the harvest date should match the observed harvest yield ($CS_{yield,obs}$) (Eq. S12).

$$CS_{yield,obs} \approx f_{cor} \sum_{t=d_{start}}^{d_{end}} CF_{gpp:grain}(t) \quad (S12)$$

130 where f_{cor} (<1) is the correction factor that takes into account the loss of carbon due to the maintenance and growth respiration of the grain. We assume that daily grain filling flux follows the right half of a downward-opening parabola, i.e., higher (lower) flux at the beginning (end) of the grain filling stage:

$$CF_{gpp:grain}(t) \approx CS_{yield,obs} / f_{cor} \cdot a((d_{end} - d_{start})^2 - (t - d_{start})^2) \quad (S13)$$

where a is a coefficient that makes $\sum_{t=d_{start}}^{d_{end}} (a((d_{end} - d_{start})^2 - (t - d_{start})^2)) = 1$.

Methods S2: Input and output of SPY-C

1. Meteorological forcing

All the input meteorological variables needed for running SPY-C are listed in Table S1 in the Supplement. They are hourly solar radiation, temperature, precipitation, surface pressure, wind, relative humidity, and CO_2 concentration. Using these variables, the vapor pressure deficit (VPD) needed by Phydro can also be derived using the improved Magnus formula (Huang, 2018) (see Eq. S14).

$$VPD = 610.94e^{17.625T/(T+243.04)} \cdot (1 - q_r) \quad (S14)$$

where q_r is relative humidity, T is air temperature ($^{\circ}C$).

2. Phenological data

In SPY-C, the annual cycle of LAI is prescribed to represent the leaf phenology of a crop. Such data can be obtained from either remote-sensed LAI products (Gasol et al., 2021) or field measurements. For cereal crops, the grain filling flux as illustrated in Eq. S13 is also prescribed as an input variable in the current version of SPY-C.

3. Crop management data

Crop management is currently implemented in its simplest form in the PA module of SPY-C. The management types considered are harvest, organic fertilization, and grazing. Only the direct effects of these managements on carbon input and output are considered and sent to the model as input data. They can be estimated according to what farmers have reported and some simple conversion factors from literature. For instance, if harvest yield is reported, the amount of carbon harvested will be removed from the existing leaf (CS_{leaf}) or grain (CS_{grain}) carbon pools depending on crop types. If the application of organic fertiliser is reported, the carbon content and the corresponding carbon fractions will be estimated and added as input to the YASSO model. Grazing management is assumed to increase carbon input to soil by producing manure and urine and reduce the amount of leaf carbon (CS_{leaf}) by feeding on plant leaf in the field. Such impacts can be estimated according to the reported number of livestock and the assumptions on the daily waste production and food consumption of the individual animal. Other common management practices, such as inorganic fertilisation and tillage, are not represented in the current model version of SPY-C simply due to the lack of necessary processes, such as the nitrogen cycle.

4. Model parameter files

The basic control settings, such as the starting and ending date of the model simulation, and all the crop and soil-related parameters are kept as namelist files in SPY-C, which are read in as input data at the beginning of the model simulation. All the parameters used in SPY-C and their values are listed in Table S2.

5. Model output data

The main output of SPY-C are variables related to carbon and water fluxes, such as GPP , $RECO$, NEE and ET , as well as carbon and water storages of plants and soil etc. A variety of optional output variables providing insight into each individual process, such as V_{cmax} and g_s , can also be added to the output for more detailed analyses. Depending on the settings, the output variables can be saved both in the hourly and daily time steps. All the outputs of SPY-C are in NetCDF format.

Methods S3: Analyses of root-zone available water at the GRASS and OAT sites.

As illustrated in Figure S1, SPY-C reproduces the observed surface soil moisture dynamics at both the GRASS and OAT site well, implying that setting soil depth to 60 cm for SpaFhy is a reasonable choice for both the GRASS and OAT site. The 60 cm soil water depth would correspond to about 270 (258) mm root-zone available water for the GRASS (OAT) site. This is at the upper limit of the root-zone available estimated in previous study Stocker et al. (2023) for this region.

To further confirm this, we use similar approaches employed by Stocker et al. (2023) to estimate the root-zone available water using observed fraction of evaporation and remote-sensed vegetation index, i.e., the red edge Chlorophyll Indices from Vira et al. (2025), and their relation to the observed cumulative water deficit. Based on the fraction of evaporation (Figure S13), we were unable to detect the root-zone available water storage for both the GRASS and OAT sites, which is likely to be much more than 100 mm.

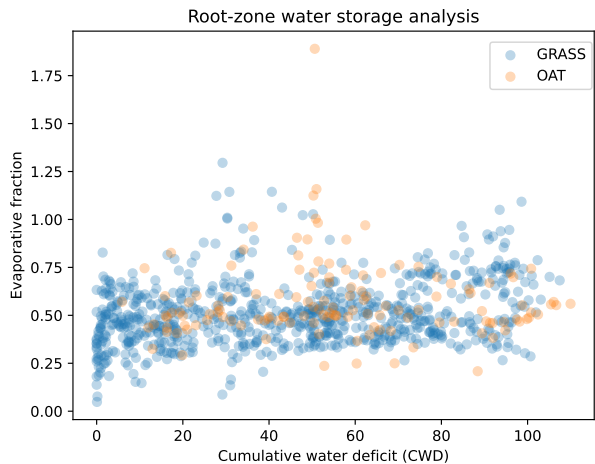


Figure S13. Root-zone available water analyses using the relation between cumulative water deficit and evaporative fraction (latent heat flux divided by absorbed solar radiation by the plant) at both the GRASS and OAT site.

Using the remote-sensed vegetation index, we are able to see that the yearly maximum red edge Chlorophyll index tends to show a negative relation with the cumulative water deficit (Figure S14). The extrapolation of such negative relation leads to an estimation of about 240 mm root-zone water storage for the GRASS site (left plot). There are only two years of observation data for the OAT site (right plot), the results are only illustrative and should not be regarded as robust.

In summary, the root-zone water storage at both study sites should be over 100 mm but likely to be less than 300 mm. The root-zone water storage assumed in our model simulations is in the upper limit of the potential range, and thus is more likely to result in a bias towards more acquisitive hydraulic strategy of the plant rather than a bias towards more conservative hydraulic strategy (cf. Figure S4 and Fig. 3), which is actually found in our results. Therefore, we consider the conservative hydraulic strategy deduced by our model simulations is not a bias of the model and its parameterization.

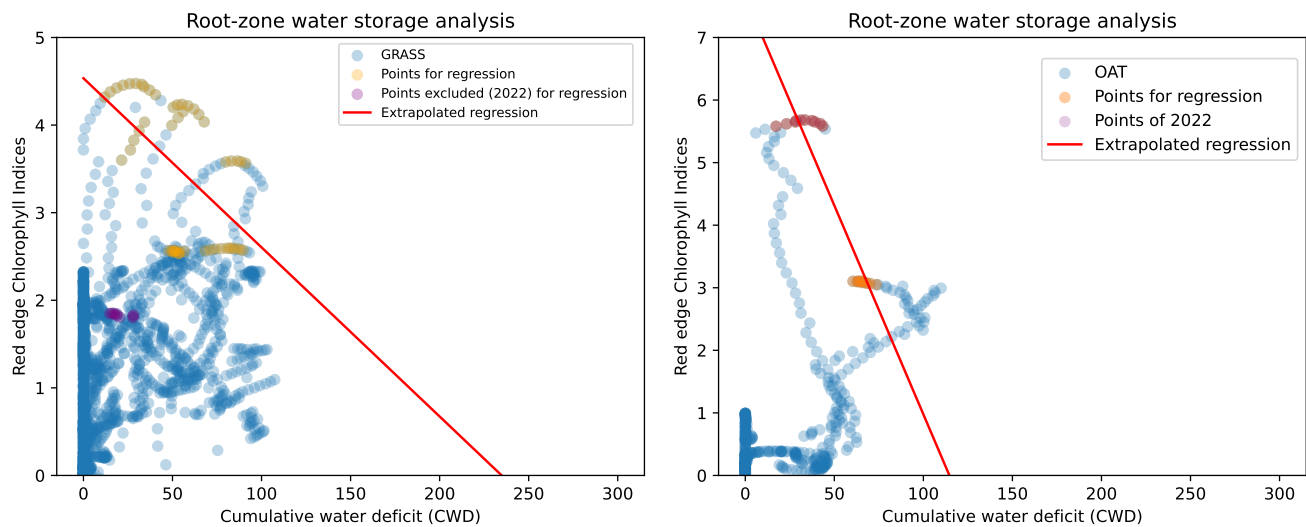


Figure S14. Root-zone available water analyses using the relation between cumulative water deficit and red edge chlorophyll indices at both the GRASS (left) and OAT (right) site.

190 **Methods S4:** The algorithm for selecting the best-fit PPE members using different benchmarking time periods.

We try to keep the algorithm for selecting the best-fit PPE members as simple as possible in this study. To do this, 4 metrics were employed. They are cor_{gpp} , $NMSE_{gpp}$, cor_{et} and $NMSE_{et}$. In the algorithm, the PPE members were firstly ranked in a descending (ascending) order according to cor_{gpp} and cor_{et} ($NMSE_{gpp}$ and $NMSE_{et}$), respectively. The search then started from the highest cor and lowest $NMSE$ one by one to see if there were PPE members that show the highest cor but the lowest $NMSE$ at the same time. The search stopped when 5 PPE members that met the criteria were found (See the following code in python).

```
for n in range(0,256):
200   index_gpp=numpy.intersect1d(sorted_cor_gpp[n],sorted_NMSE_gpp[n])
   index_et=numpy.intersect1d(sorted_cor_et[n],sorted_NMSE_et[n])
   index_bestfit=numpy.intersect1d(index_gpp,index_et)
   if numpy.size(index_bestfit)>=5:
       break
```

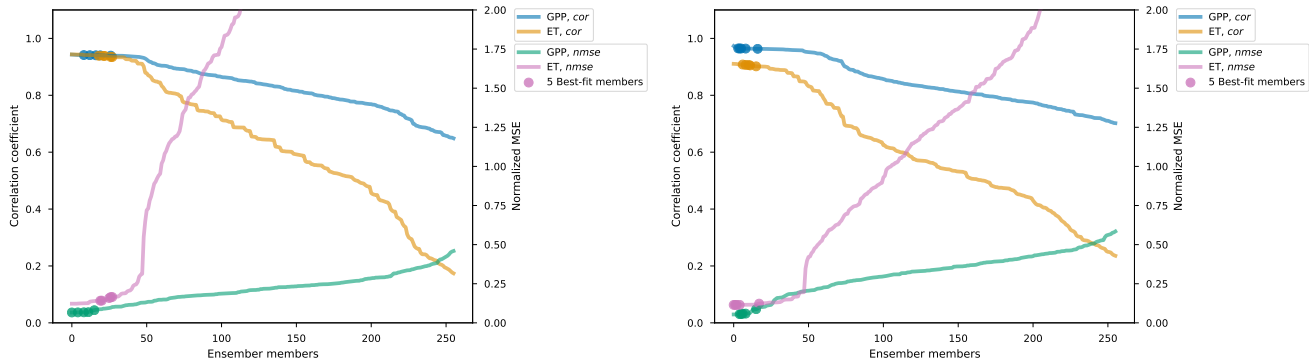


Figure S15. The position of the 5 best-fit PPE members in the sorted array of cor_{gpp} , $NMSE_{gpp}$, cor_{et} and $NMSE_{et}$ for the GRASS site (left) and the OAT site (right).

205 Figure S15 shows that the 5 best-fit PPE members are all located near each other at the near optimal positions of the 4 metrics without large trade-off. They are thus representative and robust.

To further explore the impact of using different benchmarking time periods for selecting the best-fit PPE members and the transferability of the selected best-fit PPE members to other time periods, we tested the selection procedures introduced in Sect. 2.2.3 by using observation data from each month of the growing seasons, each summer season (June-August), each growing season (May-October), or the entire observation period (2019-2022), respectively. The five best-fit simulations were then evaluated against observation from other months and years using the evaluation metrics (i.e., cor and $NMSE$). The results for QV_ctrl and HA_ctrl are shown in Fig. S16 and S17, respectively.

210 It is shown that the best-fit PPE members selected according to the observation from only May or October exhibits relatively low cor (light color rows), and high $NMSE$ (dark purple rows) for both GPP and ET suggesting a lower performance than that selected according to the observation from other months or time periods.

215 It is also noticed that the modelled GPP shows lower cor with the observation in July and August than in other months (the light color column in Fig. S16a), and the modelled ET shows lower cor and higher $NMSE$ in October (Fig. S16b and d), no matter which benchmarking time periods were used for selecting the best-fit PPE members. In contrast, the high cor and low $NMSE$ in simulating GPP and ET flux for the entire observation period (2019-2022) (see the column "ALL" in Fig. S16) can be achieved as long as the model is calibrated with observation from one summer month or season. This indicates that using

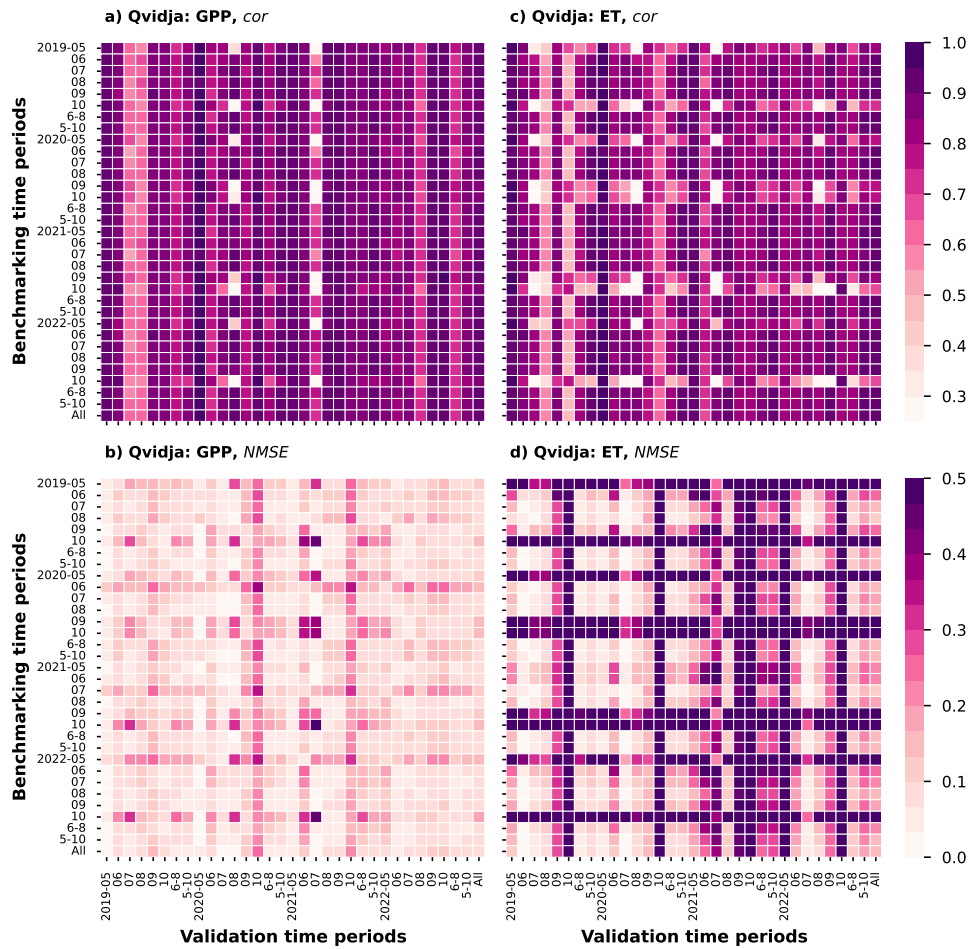


Figure S16. The performance matrices (i.e., the ensemble mean of cor and $NMSE$) of the 5 best-fit PPE members of QV_ctrl selected using different benchmarking time periods (y-axis) evaluated against the observed gross primary productivity (GPP) and evapotranspiration (ET) from different time periods (x-axis). (a) and (b) are the correlation coefficient (cor), and normalized mean square error ($NMSE$) against the observation of GPP, (c) and (d) are cor and $NMSE$ against the observation of ET.

only short summer periods of flux measurements to calibrate the four P-hydro parameters can be sufficient for SPY-C to obtain high forecasting skill in a crop field.

The ensemble mean evaluation metrics of the best-fit simulations in Hauho show quite similar pattern (Fig. S17), except that the observed GPP in September and October appears to be more challenging to simulate, because the main crop was harvested and the cover crop started to grow.

225

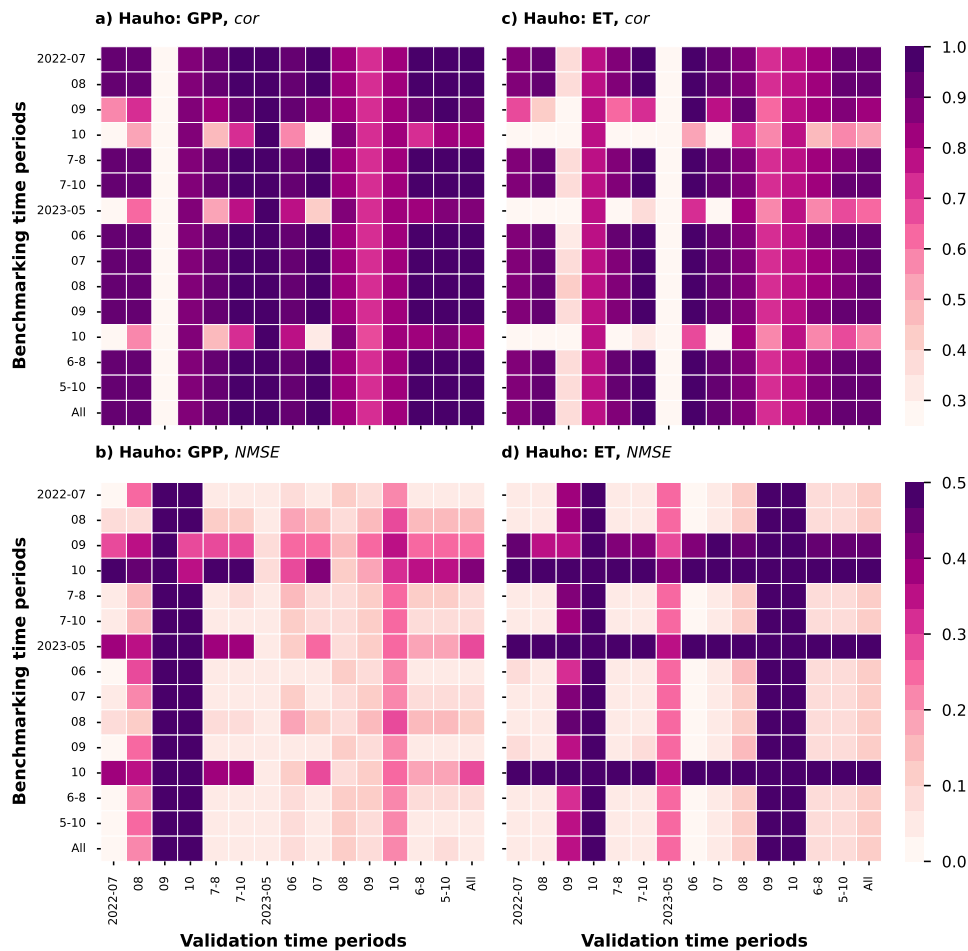


Figure S17. Same as Fig. S16 but for Hauho (HA_ctrl).

References

- CLM5.0 Technical Description of the Community Land Model (CLM5.0), Tech. Rep. NCAR/TN-417+STR, National Center for Atmospheric Research, Boulder, CO, 2018.
- Ahmad, H. B., Lens, F., Capdeville, G., Burlett, R., Lamarque, L. J., and Delzon, S.: Intraspecific Variation in Embolism Resistance and Stem Anatomy across Four Sunflower (*Helianthus Annuus* L.) Accessions, *Physiologia Plantarum*, 163, 59–72, <https://doi.org/10.1111/ppl.12654>, 2018.
- Canales, F. J., Rispail, N., García-Tejera, O., Arbona, V., Pérez-de-Luque, A., and Prats, E.: Drought Resistance in Oat Involves ABA-mediated Modulation of Transpiration and Root Hydraulic Conductivity, *Environmental and Experimental Botany*, 182, 104333, <https://doi.org/10.1016/j.envexpbot.2020.104333>, 2021.
- Corso, D., Delzon, S., Lamarque, L. J., Cochard, H., Torres-Ruiz, J. M., King, A., and Brodribb, T.: Neither Xylem Collapse, Cavitation, or Changing Leaf Conductance Drive Stomatal Closure in Wheat, *Plant, Cell & Environment*, 43, 854–865, <https://doi.org/10.1111/pce.13722>, 2020.
- Fu, Z., Ciais, P., Wigneron, J.-P., Gentile, P., Feldman, A. F., Makowski, D., Viovy, N., Kemanian, A. R., Goll, D. S., Stoy, P. C., Prentice, I. C., Yakir, D., Liu, L., Ma, H., Li, X., Huang, Y., Yu, K., Zhu, P., Li, X., Zhu, Z., Lian, J., and Smith, W. K.: Global Critical Soil Moisture Thresholds of Plant Water Stress, *Nature Communications*, 15, 4826, <https://doi.org/10.1038/s41467-024-49244-7>, 2024.

- Gaso, D. V., de Wit, A., Berger, A. G., and Kooistra, L.: Predicting Within-Field Soybean Yield Variability by Coupling Sentinel-2 Leaf Area Index with a Crop Growth Model, *Agricultural and Forest Meteorology*, 308–309, 108553, <https://doi.org/10.1016/j.agrformet.2021.108553>, 2021.
- 245 Gleason, S. M., Nalezny, L., Hunter, C., Bensen, R., Chintamanani, S., and Comas, L. H.: Growth and Grain Yield of Eight Maize Hybrids Are Aligned with Water Transport, Stomatal Conductance, and Photosynthesis in a Semi-Arid Irrigated System, *Physiologia Plantarum*, 172, 1941–1949, <https://doi.org/10.1111/ppl.13400>, 2021.
- Holloway-Phillips, M.-M. and Brodribb, T. J.: Contrasting Hydraulic Regulation in Closely Related Forage Grasses: Implications for Plant Water Use, *Functional Plant Biology*, 38, 594–605, <https://doi.org/10.1071/FP11029>, 2011a.
- 250 Holloway-Phillips, M.-M. and Brodribb, T. J.: Minimum Hydraulic Safety Leads to Maximum Water-Use Efficiency in a Forage Grass, *Plant, Cell & Environment*, 34, 302–313, <https://doi.org/10.1111/j.1365-3040.2010.02244.x>, 2011b.
- Holste, E. K., Jerke, M. J., and Matzner, S. L.: Long-Term Acclimatization of Hydraulic Properties, Xylem Conduit Size, Wall Strength and Cavitation Resistance in *Phaseolus Vulgaris* in Response to Different Environmental Effects, *Plant, Cell & Environment*, 29, 836–843, <https://doi.org/10.1111/j.1365-3040.2005.01454.x>, 2006.
- 255 Huang, J.: A Simple Accurate Formula for Calculating Saturation Vapor Pressure of Water and Ice, <https://doi.org/10.1175/JAMC-D-17-0334.1>, 2018.
- Jacob, V., Choat, B., Churchill, A. C., Zhang, H., Barton, C. V. M., Krishnananthaselvan, A., Post, A. K., Power, S. A., Medlyn, B. E., and Tissue, D. T.: High Safety Margins to Drought-Induced Hydraulic Failure Found in Five Pasture Grasses, *Plant, Cell & Environment*, 45, 1631–1646, <https://doi.org/10.1111/pce.14318>, 2022.
- 260 Johnson, K. M., Jordan, G. J., and Brodribb, T. J.: Wheat Leaves Embolized by Water Stress Do Not Recover Function upon Rewatering, *Plant, Cell & Environment*, 41, 2704–2714, <https://doi.org/10.1111/pce.13397>, 2018.
- Lamarque, L. J., Delzon, S., Toupes, H., Gravel, A.-I., Corso, D., Badel, E., Burlett, R., Charrier, G., Cochard, H., Jansen, S., King, A., Torres-Ruiz, J. M., Pouzoulet, J., Cramer, G. R., Thompson, A. J., and Gambetta, G. A.: Over-Accumulation of Abscissic Acid in Transgenic Tomato Plants Increases the Risk of Hydraulic Failure, *Plant, Cell & Environment*, 43, 548–562, <https://doi.org/10.1111/pce.13703>, 2020.
- 265 Lombardozi, D. L., Lu, Y., Lawrence, P. J., Lawrence, D. M., Swenson, S., Oleson, K. W., Wieder, W. R., and Ainsworth, E. A.: Simulating Agriculture in the Community Land Model Version 5, *Journal of Geophysical Research: Biogeosciences*, 125, e2019JG005529, <https://doi.org/10.1029/2019JG005529>, 2020.
- Matzner, S. L., Rettedal, D. D., Harmon, D. A., and Beukelman, M. R.: Constraints to Hydraulic Acclimation under Reduced Light in Two Contrasting *Phaseolus Vulgaris* Cultivars, *Journal of Experimental Botany*, 65, 4409–4418, <https://doi.org/10.1093/jxb/eru212>, 2014.
- 270 Rasmusson, L. M., Gullström, M., Gunnarsson, P. C. B., George, R., and Björk, M.: Estimation of a Whole Plant Q10 to Assess Seagrass Productivity during Temperature Shifts, *Scientific Reports*, 9, 12667, <https://doi.org/10.1038/s41598-019-49184-z>, 2019.
- Schell, V., Kervroëdan, L., Corso, D., N'do, D. Y., Faucon, M.-P., and Delzon, S.: Greater Resistance to Drought-Induced Embolism Is Linked to Higher Yield Maintenance in Soybean, *Plant, Cell & Environment*, <https://doi.org/10.1111/pce.15538>, 2025.
- Skelton, R. P., Brodribb, T. J., and Choat, B.: Casting Light on Xylem Vulnerability in an Herbaceous Species Reveals a Lack of Segmentation, *New Phytologist*, 214, 561–569, <https://doi.org/10.1111/nph.14450>, 2017.
- 275 Stocker, B. D., Tumber-Dávila, S. J., Konings, A. G., Anderson, M. C., Hain, C., and Jackson, R. B.: Global Patterns of Water Storage in the Rooting Zones of Vegetation, *Nature Geoscience*, 16, 250–256, <https://doi.org/10.1038/s41561-023-01125-2>, 2023.
- Sun, Q., Gilgen, A. K., Signarbieux, C., Klaus, V. H., and Buchmann, N.: Cropping Systems Alter Hydraulic Traits of Barley but Not Pea Grown in Mixture, *Plant, Cell & Environment*, 44, 2912–2924, <https://doi.org/10.1111/pce.14054>, 2021.
- 280 Vira, J., Vekuri, H., Nevalainen, O., Korkiakoski, M., Mattila, T., Aaltonen, H., Koskinen, M., Lohila, A., Pihlatie, M., and Liski, J.: Improving Agricultural Carbon Monitoring with Sentinel-2 and Eddy-Covariance-Based Plant Productivity Estimates, *Carbon Management*, 16, 2568042, <https://doi.org/10.1080/17583004.2025.2568042>, 2025.
- Westermann, S. A., Hildebrandt, A., Bousetta, S., and Thober, S.: Does Dynamically Modeled Leaf Area Improve Predictions of Land Surface Water and Carbon Fluxes? Insights into Dynamic Vegetation Modules, *Biogeosciences*, 21, 5277–5303, <https://doi.org/10.5194/bg-21-5277-2024>, 2024.
- 285 Xia, J., Chen, Y., Yuan, W., and Wang, Y.-P.: The Effects of Multiple Environmental Factors on Global Carbon Allocation, *Ecological Processes*, 12, 60, <https://doi.org/10.1186/s13717-023-00477-2>, 2023.